

Enhancing Quality for HEVC Compressed Videos

Ren Yang, *Student Member, IEEE*, Mai Xu, *Senior Member, IEEE*,
 Zulin Wang, *Member, IEEE*, and Zhenyu Guan

Abstract—The latest High Efficiency Video Coding (HEVC) standard has been increasingly applied to generate video streams over the Internet. However, HEVC compressed videos may incur severe quality degradation, particularly at low bit-rates. Thus, it is necessary to enhance the visual quality of HEVC videos at the decoder side. To this end, this paper proposes a Quality Enhancement Convolutional Neural Network (QE-CNN) method that does not require any modification of the encoder to achieve quality enhancement for HEVC. In particular, our QE-CNN method learns QE-CNN-I and QE-CNN-P models to reduce the distortion of HEVC I and P frames, respectively. The proposed method differs from the existing CNN-based quality enhancement approaches, which only handle intra-coding distortion and are thus not suitable for P frames. Our experimental results validate that our QE-CNN method is effective in enhancing quality for both I and P frames of HEVC videos. To apply our QE-CNN method in time-constrained scenarios, we further propose a Time-constrained Quality Enhancement Optimization (TQEO) scheme. Our TQEO scheme controls the computational time of QE-CNN to meet a target, meanwhile maximizing the quality enhancement. Next, the experimental results demonstrate the effectiveness of our TQEO scheme from the aspects of time control accuracy and quality enhancement under different time constraints. Finally, we design a prototype to implement our TQEO scheme in a real-time scenario.

Index Terms—HEVC, quality enhancement, convolutional neural network

I. INTRODUCTION

THE High Efficiency Video Coding (HEVC) standard [1] was officially issued in January 2013, and it has significantly improved the efficiency of video coding. HEVC is able to achieve a bit-rate saving of approximately 60% with similar subjective quality [2] compared with the previous H.264/AVC standard. However, when stored or transmitted at low bit-rates, HEVC videos also incur artifacts, such as blocking artifacts, ringing effects, blurring, and so forth. Such artifacts may cause severe degradation in the Quality of Experience (QoE) at the decoder side. Therefore, it is necessary to investigate how to enhance the visual quality of HEVC videos at the decoder side.

Over the past decade, there have been increasing interests in enhancing the visual quality of decoded images [3]–[10]. Recently, deep learning approaches have been successfully applied in enhancing the visual quality of decoded images. For example, Dong *et al.* [9] designed a four-layer Convolutional Neural Network (CNN) [11], named AR-CNN, for significantly improving the quality of JPEG images. Wang *et al.* [10] developed another deep network, called \mathbf{D}^3 , for enhancing the quality of JPEG images. However, to the best

Ren Yang, Mai Xu, Zulin Wang and Zhenyu Guan are with Beihang University, China. This work is supported by NSFC under Grant number 61573037. Mai Xu is the corresponding author of this paper (e-mail: Maixu@buaa.edu.cn).

of our knowledge, few works exist on enhancing the visual quality of decoded videos, particularly for HEVC videos. The closest studies on enhancing the quality of decoded videos are [12]–[15], which develop advanced postprocessing filters for the HEVC encoder. In particular, the HEVC postprocessing works of [14], [15] benefit from the most recent success of CNN. In [14], Park and Kim designed a CNN to replace the Sample Adaptive Offset (SAO) filter in the HEVC encoder and decoder. Later, based on AR-CNN [9], Dai *et al.* [15] proposed a type of CNN structure, named VRCNN, to replace the in-loop filters in HEVC intra-coding, achieving a 4.6% reduction in bit-rate.

However, [15] only handles the intra-mode coding of HEVC, in which the distortions of inter-coding frames, e.g., P frames, are not taken into consideration. More importantly, all the existing postprocessing approaches require modification at the encoder side; thus, such approaches are not suitable for enhancing visual quality when only HEVC decoded videos are available. In this paper, we propose a Quality Enhancement CNN (QE-CNN) for enhancing the visual quality of HEVC videos at the decoder side. The proposed QE-CNN method has the ability to extract features of both HEVC intra- and inter-coding. Consequently, QE-CNN is suitable for enhancing the quality of both I and P frames. Moreover, it is worth pointing out that the HEVC encoder does not need to be modified when applying our QE-CNN method at the decoder side.

Nevertheless, the cost of visual quality enhancement is increased computational time [9], [15], particularly for CNN-based approaches. Currently, the computational capacity of devices has dramatically improved, thus enabling video quality enhancement. However, the computational time is still limited for quality enhancement of HEVC, especially in real-time applications or for devices with low computational capacity. It is thus desirable to consider a time constraint when applying our QE-CNN method to enhance video quality for HEVC. To this end, we further propose a Time-constrained Quality Enhancement Optimization (TQEO) scheme. Specifically, we model the problem of TQEO by a formulation in which the quality enhancement of QE-CNN is maximized under the constraint of computational time. Then, two solutions are developed to solve our formulation for I and P frames, respectively. Consequently, the computational time of our QE-CNN method can be controlled to a target with optimal quality enhancement.

To our best knowledge, our QE-CNN method is the first CNN-based method designed to reduce the artifacts of both intra- and inter-coding frames. Our TQEO scheme is also the pioneering work to control the computational time of quality enhancement. This paper is an extended version of our conference paper [16] presented in ICME 2017, with extensive

advanced works. The extension is summarized as follows. 1) The QE-CNN model is advanced by adopting Parametric Rectified Linear Unit (PReLU) and residual learning, to achieve better quality performance on both I and P frames than [16]. 2) The TQEo scheme is further developed to control the computational time of our QE-CNN method in quality enhancement. 3) A prototype is designed to apply our TQEo scheme in a real-time quality enhancement scenario.

II. RELATED WORKS

A. Related works for quality enhancement

As mentioned above, over the past decade, many works [3]–[8] have focused on enhancing the visual quality of images. Specifically, the method proposed by Liew *et al.* [3] reduces blocking artifacts of compressed images using an overcomplete wavelet representation. Foi *et al.* [4] applied pointwise Shape-Adaptive Discrete Cosine Transform (SA-DCT) to reduce blocking and ringing effects caused by JPEG compression. Later, Wang *et al.* [8] proposed filtering the boundaries between neighboring blocks for reducing blocky artifacts of JPEG images. Recently, Jancsary *et al.* [5] achieved JPEG image deblocking by taking advantage of Regression Tree Fields (RTF). Moreover, some sparse coding methods exist for removing JPEG artifacts, such as [6] and [7].

Over the past decade, deep learning has made impressive achievements in computer vision and image processing tasks [17]–[20]. Recently, deep learning has also been successfully applied to improve the visual quality of decoded images. Dong *et al.* [9] proposed the four-layer AR-CNN to reduce the artifacts caused by JPEG coding. AR-CNN is designed based on a three-layer CNN used for super resolution, called SR-CNN [21]. In [21], the functions of the three layers in SRCNN are defined as feature extraction, non-linear mapping and reconstruction. AR-CNN adds a feature denoising layer to SR-CNN to extract the features of JPEG distortion, thereby achieving quality enhancement on JPEG images. Then, \mathbf{D}^3 , another deep network for JPEG image restoration, was proposed by Wang *et al.* in [10]. \mathbf{D}^3 restores the JPEG distortion by utilizing the prior knowledge of JPEG compression. As reported in [9], [10], these deep learning approaches significantly outperform other conventional methods, such as [4]–[6]. The outstanding performance of [9], [10] highlights the promising application of deep learning in quality enhancement.

For videos, many works [12]–[15], [22], [23] have been conducted to improve visual quality for the latest HEVC standard, aiming at improving the coding efficiency at the encoder side. The works of [22] and [23] propose to improve the HEVC quality by Rate-Distortion Optimization (RDO) at the HEVC encoder. Han *et al.* [12] developed a high-performance in-loop filter for HEVC, which is added after the original in-loop filter in the HEVC encoder and decoder. Consequently, the visual quality of encoded videos can be slightly improved over the conventional HEVC standard, equivalent to saving 2% bit-rate on average. Zhang *et al.* [13] proposed a Structure-driven Adaptive Non-local Filter (SANF), which is applied after the Deblocking Filter (DF) and before the SAO filter at both the HEVC encoder and decoder sides. Park and Kim

[14] proposed replacing the SAO filter in HEVC by the re-trained SR-CNN [21] to enhance the quality of HEVC videos. Later, based on AR-CNN [9], Dai *et al.* [15] proposed the VRCNN as an advanced in-loop filter in HEVC intra-coding. The VRCNN enhances the visual quality of HEVC without any increase in bit-rate compared with the conventional in-loop filters of HEVC. In other words, VRCNN is able to improve the coding efficiency of HEVC, i.e., a 4.6% bit-rate reduction. It has been verified that VRCNN [15] performs better than other non-CNN methods, further demonstrating the feasibility of deep learning in enhancing the quality of encoded videos. Nevertheless, few works concentrate on enhancing the visual quality of decoded videos, which can be directly applied to the existing video streams. Moreover, little attention has been devoted to exploring patterns of temporal distortion for further enhancing the visual quality of inter-frames (i.e., B and P frames).

B. Related works on HEVC complexity control

To the best of our knowledge, no works on controlling the computational time for video quality enhancement exist. The closest works are HEVC complexity control approaches, which aim at making the encoding or decoding time of HEVC meet a constraint. Specifically, at the encoder side, Corrêa *et al.* [24] proposed reducing the HEVC encoding complexity by skipping the computation on the Coding Tree Unit (CTU) partition at some frames. Instead, the CTU partitions of these frames are the same as those of previous frames. Then, the encoding complexity can be controlled by setting the number of frames that skip computation on the CTU partition. Later, Deng *et al.* [25], [26] proposed a complexity control approach for HEVC encoding. In their approach, the maximal depths of some CTUs are limited to reduce the computational complexity to a target with minimal quality loss.

At the decoder side, Langroodi *et al.* [27] developed a complexity control approach for H.264/AVC decoding. In [27], the decoder sends its computational resource demand to the encoder side. Then, the settings of the encoder are adjusted according to the received demand such that the corresponding decoding complexity can be controlled. Rather than adjusting the encoder, Yang *et al.* [28], [29] proposed an approach for controlling the HEVC decoding complexity. In their approach, the decoding complexity of HEVC is reduced by disabling DF and simplifying Motion Compensation (MC) at the expense of quality loss. Then, the HEVC decoding complexity is controlled to a certain target with minimal perceptual quality loss by disabling DF and simplifying the MC of non-salient CTUs. Similar to the above approaches, computational time control can also be studied for video quality enhancement under a time constraint. Unfortunately, to the best of our knowledge, there exists no work in this direction.

III. THE PROPOSED QUALITY ENHANCEMENT METHOD

In this section, we discuss the proposed QE-CNN method for enhancing the quality of decoded HEVC videos. In Section III-A, we briefly review the overall architecture of AR-CNN, which is the basis of our QE-CNN method. In Sections III-B

and III-C, we introduce the proposed network architecture of our QE-CNN method in detail, including QE-CNN-I for enhancing the visual quality of HEVC I frames and QE-CNN-P designed for HEVC P frames.

A. Overview of AR-CNN

In [9], AR-CNN is developed to improve the visual quality of encoded JPEG images. AR-CNN achieves a quality improvement on JPEG encoded images, and it can be viewed as the foundation of our method. Here, we briefly review the architecture of AR-CNN.

TABLE I
CONFIGURATION OF AR-CNN [9]

| Layer index | Conv 1 | Conv 2 | Conv 3 | Conv 4 |
|-------------------|--------------|--------------|--------------|--------------|
| Filter size | 9×9 | 7×7 | 1×1 | 5×5 |
| Filter number | 64 | 32 | 16 | 1 |
| W learning rate | 10^{-4} | 10^{-4} | 10^{-4} | 10^{-5} |
| B learning rate | 10^{-5} | 10^{-5} | 10^{-5} | 10^{-5} |

In AR-CNN, there are four convolutional layers without any pooling or fully connected layers. Specifically, as presented in [9], the four layers of AR-CNN perform the functions of feature extraction, feature denoising, non-linear mapping and reconstruction. AR-CNN is designed as an end-to-end framework, which takes the JPEG compressed images as input and directly outputs the restored images. During training, all four layers of AR-CNN are jointly optimized.

The input image is denoted as \mathbf{Y} , and the output of the i -th convolutional layer is defined as $F_i(\mathbf{Y})$. Then, the architecture of AR-CNN can be expressed as

$$F_0(\mathbf{Y}) = \mathbf{Y}, \quad (1)$$

$$F_i(\mathbf{Y}) = \max(0, W_i * F_{i-1}(\mathbf{Y}) + B_i), \quad i \in \{1, 2, 3\}, \quad (2)$$

$$F_4(\mathbf{Y}) = W_4 * F_3(\mathbf{Y}) + B_4, \quad (3)$$

where W_i and B_i are the weights and bias matrices of the i -th layer, respectively, and $*$ indicates the convolution operator. Note that $\max(0, x)$, known as Rectified Linear Unit (ReLU), is adopted in the first three layers as the non-linear activation function. The configuration of AR-CNN is summarized in Table I.

The experimental results reported in [9] verify that AR-CNN has better performance than conventional methods, e.g., SA-DCT [4] and RTF [5], for improving the quality of encoded images. Inspired by AR-CNN, we design QE-CNN for enhancing the quality of HEVC decoded videos, also taking advantage of the CNN.

B. The proposed QE-CNN-I

We now focus on the proposed network of QE-CNN-I, which is able to handle distortion caused by intra-coding of HEVC, for enhancing the quality of HEVC I frames. Next, we present QE-CNN-I from the aspects of dataset, architecture and loss function.

Dataset. First, we establish a dataset for learning QE-CNN-I. In our work, the images of our training and validation sets for QE-CNN-I are the same as AR-CNN [9], which are

TABLE II
CONFIGURATION AND PERFORMANCE OF AR-CNN AND AR-CNN-1/2/3.

| Network | AR-CNN | AR-CNN-1 | AR-CNN-2 | AR-CNN-3 |
|--------------------|------------|-------------|----------------|----------------|
| Filter size | 9-7-1-5 | 9-7-1-5 | 9-7-3-1-5 | 9-7-3-1-5 |
| Filter number | 64-32-16-1 | 128-64-32-1 | 128-64-64-32-1 | 128-64-64-32-1 |
| Function | ReLU | ReLU | ReLU | PReLU |
| Δ PSNR (dB) | 0.2058 | 0.2203 | 0.2425 | 0.2487 |

selected from the BSDS500 database [30]. Because QE-CNN-I aims to reduce the distortion of I frames in HEVC, we encode all training images using the HEVC all intra (AI) mode at $QP = 32, 37, 42$ and 47 using the default configuration in *encoder_intra_main.cfg*. Before training, we decompose the ground-truth and HEVC encoded images into image patches with a size of 40×40 , using a stride of 10. Consequently, the training set with 400 images provides a total of 522,000 pairs of training samples. Similarly, 34,500 pairs of validation samples are obtained.

Architecture. The architecture of QE-CNN-I is designed according to the following observations.

Observation 1. The distortion caused by HEVC intra-coding is with more features than JPEG.

Analysis 1. We analyze this observation from both theoretical and experimental aspects. Theoretically, HEVC intra-coding is more complicated compared to JPEG. For example, HEVC supports different sizes of Discrete Cosine Transform (DCT), including $4 \times 4, 8 \times 8, 16 \times 16$ and 32×32 [1], whereas JPEG only adopts 8×8 DCT [31]. Moreover, the HEVC intra-picture prediction has 33 different directional orientations [1], which is much more complex than the Direct-Current (DC) prediction in JPEG [31]. Accordingly, more distortion sources exist in HEVC intra-coding than in JPEG; thus, the distortion caused by HEVC intra-coding has more features than JPEG.

From the experimental aspect, we further analyze *Observation 1* by testing CNN on the validation set under different configurations. In CNN, convolutional filters are used to extract features from input images for quality enhancement [11]. Thus, more convolutional filters should be used to handle input images with more distortion-related features. Hence, based on AR-CNN, we design AR-CNN-1 with a larger number of convolutional filters. Then, we compare the performance of AR-CNN-1 with AR-CNN at $QP = 42$ on the validation set. The configuration of AR-CNN-1 and its performance are shown in Table II. As shown in Table II, AR-CNN-I, which has more filters, performs better than AR-CNN in terms of enhancing the quality of HEVC I frames. Therefore, *Observation 1* can be verified. ■

Observation 2. AR-CNN-1 with one additional convolutional layer can extract more effective distortion-related features for HEVC, thus leading to better performance.

Analysis 2. Recall that AR-CNN is a 4-layer network, in which Conv 1 is used to extract features and Conv 2 is for feature denoising [9]. For HEVC, we extend AR-CNN-1 to AR-CNN-2, which includes one additional layer after Conv 2 to further denoise the features. The configuration of AR-CNN-2 is shown in Table II. As such, AR-CNN-2 has 5 convolutional layers. Then, we test AR-CNN-2 on the validation set at $QP = 42$. As shown in Table II, AR-CNN-2

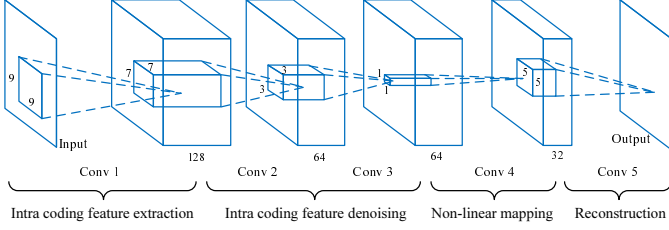


Fig. 1. Network architecture of QE-CNN-I.

TABLE III
CONFIGURATION OF QE-CNN-I.

| Layer | Conv 1 | Conv 2 | Conv 3 | Conv 4 | Conv 5 |
|-------------------|--------------|--------------|--------------|--------------|--------------|
| Filter size | 9×9 | 7×7 | 3×3 | 1×1 | 5×5 |
| Filter number | 128 | 64 | 64 | 32 | 1 |
| W learning rate | 10^{-4} | 10^{-4} | 10^{-4} | 10^{-4} | 10^{-5} |
| B learning rate | 10^{-5} | 10^{-5} | 10^{-5} | 10^{-5} | 10^{-5} |

outperforms AR-CNN-1 for HEVC quality enhancement of I frames. Therefore, it can be confirmed that Conv 3 succeeds in further denoising the feature maps for HEVC encoded images. Finally, *Observation 2* is validated. ■

Observation 3. Parametric Rectified Linear Unit (PReLU), as the activation function instead of ReLU, can further improve the performance of AR-CNN-2.

Analysis 3. PReLU is a learnable activation function, which is proved to have better performance than ReLU [32]. PReLU is defined as follows:

$$\text{PReLU}(x) = \max(0, x) + a \cdot \min(0, x), \quad (4)$$

where a is a parameter learned during the training stage. Recall that ReLU is defined as $\max(0, x)$; thus, its output always remains zero at the negative side. As a result, ReLU may incur the problem of “dead features” [33]. However, PReLU, whose slope is learnable under negative input, is able to avoid the problem of “dead features”. We further test the performance of PReLU on the validation set at $QP = 42$. As shown in Table II, AR-CNN-3, which replaces ReLU by PReLU in AR-CNN-2, has better performance than AR-CNN-2. Consequently, *Observation 3* can be validated. ■

According to *Observations 1, 2 and 3*, we use AR-CNN-3 as our QE-CNN-I structure to enhance the quality of I frames of decoded HEVC videos. The architecture of QE-CNN-I is shown in Fig. 1, and its configuration is shown in Table III. The formulation of QE-CNN-I is expressed as

$$F_0(\mathbf{Y}) = \mathbf{Y}, \quad (5)$$

$$F_i(\mathbf{Y}) = \text{PReLU}(W_i * F_{i-1}(\mathbf{Y}) + B_i), \quad i \in \{1, 2, 3, 4\}, \quad (6)$$

$$F_5(\mathbf{Y}) = W_5 * F_4(\mathbf{Y}) + B_5, \quad (7)$$

where W_i and B_i are the weights and bias matrices of the i -th layer, respectively. Note that PReLU is adopted as the non-linear activation function in the layers of Conv 1-4.

Loss function. We apply Mean Squared Error (MSE) as the loss function of our QE-CNN-I. Let $\{\mathbf{X}_n\}_{n=1}^N$ be the set of raw image patches, seen as the ground-truth, and let $\{\mathbf{Y}_n\}_{n=1}^N$ be patches of their corresponding compressed images. Here, $\{\mathbf{Y}_n\}_{n=1}^N$ are input samples, whereas $\{\mathbf{X}_n\}_{n=1}^N$

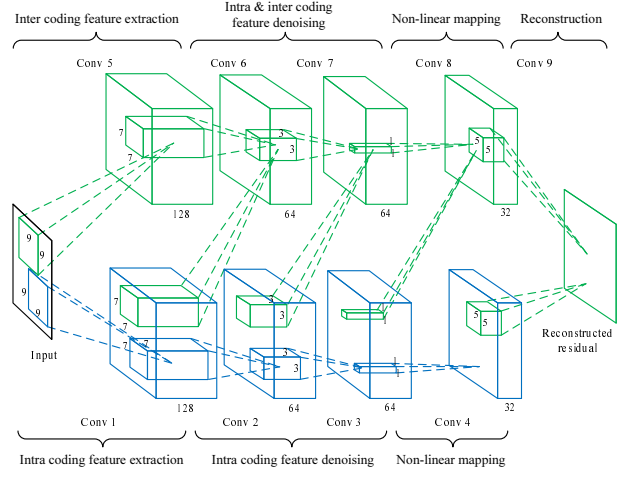


Fig. 2. Network architecture of QE-CNN-P.

TABLE IV
CONFIGURATION OF QE-CNN-P.

| Layer | Conv 1 Conv 5 | Conv 2 Conv 6 | Conv 3 Conv 7 | Conv 4 Conv 8 | Conv 9 |
|---------------|------------------|------------------|------------------|------------------|--------------|
| Filter size | 9×9 | 7×7 | 3×3 | 1×1 | 5×5 |
| Filter number | 128 | 64 | 64 | 32 | 1 |
| ILR for W | 10^{-1} | 10^{-1} | 10^{-1} | 10^{-1} | 10^{-2} |
| ILR for B | 10^{-2} | 10^{-2} | 10^{-2} | 10^{-2} | 10^{-2} |

are the corresponding target output. Define $F(\cdot)$ as the output of QE-CNN-I. Then, the loss function is as follows:

$$L(\Theta) = \frac{1}{N} \sum_{n=1}^N \|F(\mathbf{Y}_n; \Theta) - \mathbf{X}_n\|_2^2, \quad (8)$$

where $\Theta = \{W_i, B_i\}$ stands for the weights and bias in QE-CNN-I. This loss function is minimized using the stochastic gradient descent algorithm with the standard Back-Propagation (BP). We follow [9] and [15] to set the batch size as 128 when training QE-CNN-I. Note that we first train our QE-CNN-I at $QP = 42$, and the networks for the other QPs (i.e., 32, 37 and 47) are fine-tuned from $QP = 42$.

C. The proposed QE-CNN-P

Next, we introduce the proposed network of QE-CNN-P, which is designed to handle both HEVC intra- and inter-coding distortions. Therefore, it is able to enhance the quality of HEVC P frames. In the following, we present the dataset, architecture and loss function for QE-CNN-P.

Dataset. First, we establish a video database¹ that includes 89 sequences. We randomly selected 8 sequences (i.e., *ParkRun*, *Shields*, *Stockholm*, *Mobcal*, *Tennis*, *PartyScene*, *FlowerVase* and *BasketballDrill*) as our validation set for QE-CNN-P, and the other 81 sequences are used for training. Since our QE-CNN-P is implemented for enhancing the quality of P frames, all the training and validation sequences are encoded by HEVC Low-Delay P (LDP) mode at QP

¹ Available at <https://github.com/ryangBUAA/Videos.git>.

= 32, 37, 42 and 47, with the default configuration in *encoder_lowdelay_P_main.cfg*. We randomly select 10 P frames from each training sequence, and we decompose the raw and encoded frames into pairs of 40×40 image patches, with the stride being 15. In this way, we obtain 1,241,880 training sample pairs. Similarly, 279,090 validation sample pairs are obtained.

Architecture. In HEVC, only intra-picture coding is used in I frames, while both intra- and inter-coding are applied in P frames [1]. Thus, we learn the features of both HEVC intra- and inter-coding to enhance the visual quality of P frames. Accordingly, we design the QE-CNN-P containing 9 convolutional layers, as shown in Fig 2. In QE-CNN-P, the architectures of layers Conv 1-4 are the same as those in QE-CNN-I, which are expected to extract and handle the distortion features of intra-coding. Moreover, Conv 5 is used to extract the distortion features of HEVC inter-coding. Recall that Conv 1 is used to extract intra-coding features. Then, the outputs of Conv 1 and Conv 5 are concatenated, and both are convolved by Conv 6. Thus, Conv 6 denoises the features of both intra- and inter-coding. Conv 7-9 in QE-CNN-P are designed in a similar way. Finally, Conv 9 in QE-CNN-P is used for reconstruction. Note that since Conv 1-3 in QE-CNN-P are used to extract intra-coding features, their parameters are fine-tuned from Conv 1-3 of the learned QE-CNN-I.

In Conv 6-9, we define $W_i^{(1)}$ and $W_2^{(1)}$ as the weights of Conv i used to convolve the data in Conv 1-4 and Conv 5-8, respectively. $\{W_i\}_{i=1}^5$ are also defined as the weights of Conv 1-5, and $\{B_i\}_{i=1}^9$ denotes the biases of Conv 1-9. Then, the formulation of QE-CNN-P can be expressed as

$$F_0(\mathbf{Y}) = \mathbf{Y}, \quad (9)$$

$$F_i(\mathbf{Y}) = \text{PReLU}(W_i * F_{i-1}(\mathbf{Y}) + B_i), \quad i \in \{1, 2, 3, 4\}, \quad (10)$$

$$F_5(\mathbf{Y}) = \text{PReLU}(W_5 * F_0(\mathbf{Y}) + B_5), \quad (11)$$

$$F_i(\mathbf{Y}) = \text{PReLU}(W_i^{(1)} * F_{i-5}(\mathbf{Y}) + W_i^{(1)} * F_{i-1}(\mathbf{Y}) + B_i), \quad i \in \{6, 7, 8\}, \quad (12)$$

$$F_9(\mathbf{Y}) = W_9^{(1)} * F_4(\mathbf{Y}) + W_9^{(1)} * F_8(\mathbf{Y}) + B_9. \quad (13)$$

The sizes and numbers of filters at different layers in QE-CNN-P are shown in Table IV, in which ILR means initial learning rate.

Training procedure and loss function. Since QE-CNN-P contains a larger number of layers than QE-CNN-I, we use the strategy of residual learning [34] to accelerate its convergence with better results. Specifically, we use the residual between raw and encoded videos as the ground-truth for training rather than the raw video itself. Moreover, we also apply learning rate decay in training QE-CNN-P. In this paper, the learning rate decays by a factor of 10 every 40 epochs. Meanwhile, to avoid exploding caused by a large learning rate (γ), we also adopt the adjustable gradient clipping method [35]. The gradient g is clipped into the range of $g \leq |\beta/\gamma|$, where β is a parameter for restricting the gradient. We follow [35] to set the Initial Learning Rate (ILR) as $\gamma = 10^{-1}$ and set $\beta = 10^{-2}$.

For QE-CNN-P, we also apply MSE as the loss function. As residual learning is adapted in QE-CNN-P, its loss function,

which is different from QE-CNN-I, is written as follows:

$$L(\Theta) = \frac{1}{N} \sum_{n=1}^N \|F(\mathbf{Y}_n; \Theta) - (\mathbf{X}_n - \mathbf{Y}_n)\|_2^2, \quad (14)$$

where all notations are the same as in QE-CNN-I. The loss function is also minimized by stochastic gradient descent with the BP algorithm, and the batch size is set as 128. The same as QE-CNN-I, QE-CNN-P is first trained at QP = 42, and the other QPs are fine-tuned from QP = 42.

IV. EXPERIMENTAL RESULTS ON QUALITY ENHANCEMENT

In this section, experimental results are presented to validate the effectiveness of our QE-CNN method in comparison with the latest quality enhancement methods² AR-CNN [9] and VRCNN [15]. In the following, we discuss the settings of our experiments in Section IV-A, compare the performance of quality enhancement in Section IV-B, and evaluate the computational time in Section IV-C.

A. Settings

In our experiments, we test our method and the other two methods on 17 sequences from the JCT-VC [36] database. Details about the test sequences are presented in Table V. The training and validation sequences are the same as those introduced in Sections III-B and III-C. Note that the test sequences do not overlap with those of the training and validation sets. For each sequence, the corresponding HEVC bitstream is generated by HM 16.0 with LDP mode at four QP values (i.e., 32, 37, 42 and 47). Here, the default configuration file *encoder_lowdelay_P_main.cfg* is used. Then, our QE-CNN method and the AR-CNN and VRCNN methods are applied to enhance the quality of the encoded HEVC sequences. Note that for a fair comparison, AR-CNN and VRCNN are re-trained on HEVC using the same training samples as our QE-CNN method. Recall that the hyperparameters of our QE-CNN method, e.g., learning rate, batch size, and so forth, are introduced in Section III.

B. Performance of quality enhancement

We now evaluate the performance of our QE-CNN method in terms of quality enhancement, comparing with the conventional AR-CNN [9] and VRCNN [15]. The quality enhancement is measured by Y-PSNR improvement (Δ PSNR), and the Δ PSNR results of our method and the other two methods are reported in Table V.

Quality enhancement on I frames. As shown in Table V, the proposed QE-CNN-I model clearly outperforms AR-CNN and VRCNN on I frames over all test sequences. At QP = 42, the average Δ PSNR (0.3469 dB) of our QE-CNN-I model is 38.58% higher than that of AR-CNN (0.2503 dB) and 28.82% higher than that of VRCNN (0.2693 dB). In particular, QE-CNN-I has up to a 0.5065 dB Y-PSNR improvement on I frames, which is achieved in the sequence *KristenAndSara*.

²Here, we do not compare with \mathbf{D}^3 [10]. It is because \mathbf{D}^3 , which is designed according to prior knowledge of JPEG, cannot be implemented in HEVC.

TABLE V
 Δ PSNR (dB) OF OUR QE-CNN, AR-CNN [9] AND VRCNN [15] METHODS AT QP = 42 / 32.

| QP | Class | Sequence | VRCNN [15] | | AR-CNN [9] | | QE-CNN-I | | QE-CNN-P | |
|---------|----------------|------------------------|-----------------|-----------------|-----------------|------------------------|-----------------|------------------------|----------|--|
| | | | I frames | I frames | P frames | I frames | P frames | P frames | P frames | |
| 42 / 32 | A | <i>Traffic</i> | 0.2643 / 0.2537 | 0.2372 / 0.2075 | 0.1499 / 0.1138 | 0.3423 / 0.3914 | 0.2504 / 0.2540 | 0.3285 / 0.3489 | | |
| | | <i>PeopleOnStreet</i> | 0.3294 / 0.1975 | 0.2896 / 0.1854 | 0.1330 / 0.1126 | 0.4461 / 0.3735 | 0.2501 / 0.2943 | 0.5649 / 0.5515 | | |
| | B | <i>BQTerrace</i> | 0.3127 / 0.1325 | 0.3277 / 0.1103 | 0.2149 / 0.0704 | 0.4149 / 0.2199 | 0.3114 / 0.1689 | 0.3185 / 0.2160 | | |
| | | <i>Cactus</i> | 0.1754 / 0.1357 | 0.1534 / 0.1021 | 0.1159 / 0.0755 | 0.2660 / 0.2259 | 0.2185 / 0.1798 | 0.2809 / 0.2287 | | |
| | | <i>BasketballDrive</i> | 0.1776 / 0.0862 | 0.1803 / 0.0541 | 0.1351 / 0.0611 | 0.2708 / 0.1714 | 0.2284 / 0.1818 | 0.3284 / 0.2698 | | |
| | | <i>ParkScene</i> | 0.1556 / 0.1525 | 0.1064 / 0.1421 | 0.0682 / 0.0742 | 0.1608 / 0.2442 | 0.1130 / 0.1435 | 0.1782 / 0.1826 | | |
| | C | <i>Kimono</i> | 0.1386 / 0.1777 | 0.1265 / 0.1086 | 0.1066 / 0.0915 | 0.1955 / 0.2212 | 0.1675 / 0.1917 | 0.3069 / 0.2917 | | |
| | | <i>BQMall</i> | 0.2946 / 0.1517 | 0.2711 / 0.1449 | 0.1781 / 0.0968 | 0.3624 / 0.3416 | 0.2636 / 0.2394 | 0.2878 / 0.2483 | | |
| | | <i>RaceHorses</i> | 0.2663 / 0.1980 | 0.2371 / 0.1529 | 0.1572 / 0.1024 | 0.2891 / 0.2839 | 0.2114 / 0.2081 | 0.2790 / 0.2774 | | |
| | | <i>Keiba</i> | 0.2351 / 0.2196 | 0.2046 / 0.1065 | 0.1614 / 0.0937 | 0.2925 / 0.2411 | 0.2571 / 0.2111 | 0.2659 / 0.2554 | | |
| | E | <i>Mobisode</i> | 0.2616 / 0.2092 | 0.1826 / 0.1157 | 0.1843 / 0.1079 | 0.2698 / 0.2748 | 0.2386 / 0.2401 | 0.2837 / 0.3079 | | |
| | | <i>Johnny</i> | 0.2823 / 0.2077 | 0.2876 / 0.1367 | 0.1664 / 0.0899 | 0.3807 / 0.3767 | 0.2761 / 0.2795 | 0.2994 / 0.3411 | | |
| | | <i>FourPeople</i> | 0.4060 / 0.3640 | 0.3812 / 0.2592 | 0.2955 / 0.1809 | 0.4949 / 0.5486 | 0.4137 / 0.3884 | 0.4636 / 0.4817 | | |
| | | <i>KristenAndSara</i> | 0.4303 / 0.2866 | 0.4004 / 0.2146 | 0.2943 / 0.1677 | 0.5065 / 0.4732 | 0.4020 / 0.3601 | 0.4380 / 0.4324 | | |
| | E' | <i>Vidyo1</i> | 0.3619 / 0.2897 | 0.3419 / 0.2222 | 0.2289 / 0.1497 | 0.4585 / 0.4615 | 0.3466 / 0.3295 | 0.4147 / 0.4545 | | |
| | | <i>Vidyo3</i> | 0.2126 / 0.2644 | 0.2744 / 0.2114 | 0.1415 / 0.1123 | 0.3802 / 0.4576 | 0.2769 / 0.3200 | 0.4181 / 0.5053 | | |
| | | <i>Vidyo4</i> | 0.2730 / 0.2215 | 0.2528 / 0.1644 | 0.1689 / 0.1111 | 0.3655 / 0.3418 | 0.2802 / 0.2541 | 0.3361 / 0.3300 | | |
| | Average | | 0.2693 / 0.2087 | 0.2503 / 0.1552 | 0.1706 / 0.1066 | 0.3469 / 0.3328 | 0.2650 / 0.2496 | 0.3407 / 0.3367 | | |

At QP = 32, our QE-CNN-I model enhances the quality of I frames by 0.3328 dB on average, doubling the enhancement of AR-CNN (0.1552 dB). Meanwhile, the quality enhancement of QE-CNN-I is 59.44% higher than that of VRCNN (0.2087 dB). The maximum enhancement of QE-CNN-I is 0.5486 dB, which is achieved in the sequence *FourPeople*. Similar results can be found for the other QPs. To summarize, the proposed QE-CNN-I model significantly outperforms the state-of-the-art AR-CNN and VRCNN methods in enhancing the quality of I frames.

Quality enhancement on P frames. As shown in Table V, the QE-CNN-I and QE-CNN-P models both perform better than AR-CNN over P frames of all test sequences. Note that we do not compare with VRCNN over HEVC P frames because VRCNN [15] is only designed to improve the coding efficiency of HEVC intra-mode, and applying VRCNN on P frames requires modification of the HEVC encoder. Table V shows that QE-CNN-I also has the ability to enhance the quality of P frames due to the reduction in intra-coding distortion. At QP = 42, QE-CNN-I still has a 55.36% gain of Δ PSNR (0.2650 dB) over AR-CNN (0.1706 dB). Similarly, at QP = 32, the Δ PSNR of QE-CNN-I is 0.2496 dB for P frames, which is much higher than the 0.1066 dB of AR-CNN.

Furthermore, our QE-CNN-P model yields better quality than QE-CNN-I for the P frames of HEVC sequences, benefiting from its specific design in enhancing the quality of P frames. At QP = 42, QE-CNN-P reaches a 0.3407 dB Y-PSNR improvement on P frames averaged over all the test sequences, which is 28.57% higher than that of QE-CNN-I (0.2650 dB). Moreover, our QE-CNN-P model nearly doubles the performance of AR-CNN (0.1706 dB). At QP = 32, our QE-CNN-P model improves Y-PSNR by 0.3328 dB on average, which is considerably higher than that of QE-CNN-I (0.2496 dB). More importantly, the QE-CNN-P model triples the quality enhancement of AR-CNN (0.1066 dB) averaged over the P frames of all the test sequences. In other words, for the P frames of HEVC sequences, our QE-CNN-P model improves the quality enhancement performance of both AR-CNN and our QE-CNN-I model.

Subjective quality performance. Three frames are selected from *BQMall*, *Cactus* and *PeopleOnStreet* for evaluating the

subjective quality performance of our QE-CNN method and the conventional AR-CNN method. Fig. 3 shows the three frames compressed by HEVC and then enhanced by AE-CNN and QE-CNN. In this figure, the raw frames are also shown for comparison. As shown, our QE-CNN method effectively reduces the artifacts, e.g., blurring and ringing effects, caused by HEVC compression. Additionally, our QE-CNN method is clearly better than the conventional AR-CNN method in reducing HEVC compression artifacts.

Rate-distortion performance. We further evaluate the rate-distortion performance of our QE-CNN method in terms of Bjontegaard Distortion-rate (BD-rate) savings over HM 16.0 baseline. In our experiments, the BD-rate is calculated according to the Y-PSNR and bit-rates at QP = 32, 37, 42 and 47. As shown in Table VI, our QE-CNN method, which applies QE-CNN-I on I frames and QE-CNN-P on P frames, is able to save BD-rate up to 10.98%. Moreover, the average BD-rate saving is 8.31% when applying our QE-CNN method. This BD-rate saving of our QE-CNN method is considerably better than that of AR-CNN, which only has 3.69% BD-rate saving on average.

TABLE VI
BD-RATE OF OUR QE-CNN AND AR-CNN [9] METHODS OVER HM 16.0.

| Class | Sequence | AR-CNN [9] (%) | QE-CNN (%) |
|-------|------------------------|----------------|-----------------|
| A | <i>Traffic</i> | -3.7189 | -8.1475 |
| | <i>PeopleOnStreet</i> | -2.8766 | -10.9799 |
| B | <i>BQTerrace</i> | -6.0523 | -10.0620 |
| | <i>Cactus</i> | -3.2953 | -7.6003 |
| C | <i>BasketballDrive</i> | -3.4625 | -8.9742 |
| | <i>ParkScene</i> | -2.6345 | -6.2298 |
| E | <i>Kimono</i> | -3.1914 | -8.4617 |
| | <i>BQMall</i> | -3.8604 | -6.8312 |
| | <i>RaceHorses</i> | -4.4833 | -8.8032 |
| | <i>Keiba</i> | -3.8164 | -6.9734 |
| E' | <i>Mobisode</i> | -4.0902 | -7.2911 |
| | <i>Johnny</i> | -3.6559 | -7.6202 |
| | <i>FourPeople</i> | -5.4367 | -9.2597 |
| E' | <i>KristenAndSara</i> | -5.5227 | -9.0921 |
| | <i>Vidyo1</i> | -4.4038 | -8.6052 |
| | <i>Vidyo3</i> | -3.1248 | -8.8447 |
| E' | <i>Vidyo4</i> | -3.6136 | -7.4675 |
| | AVERAGE | -3.9552 | -8.3085 |

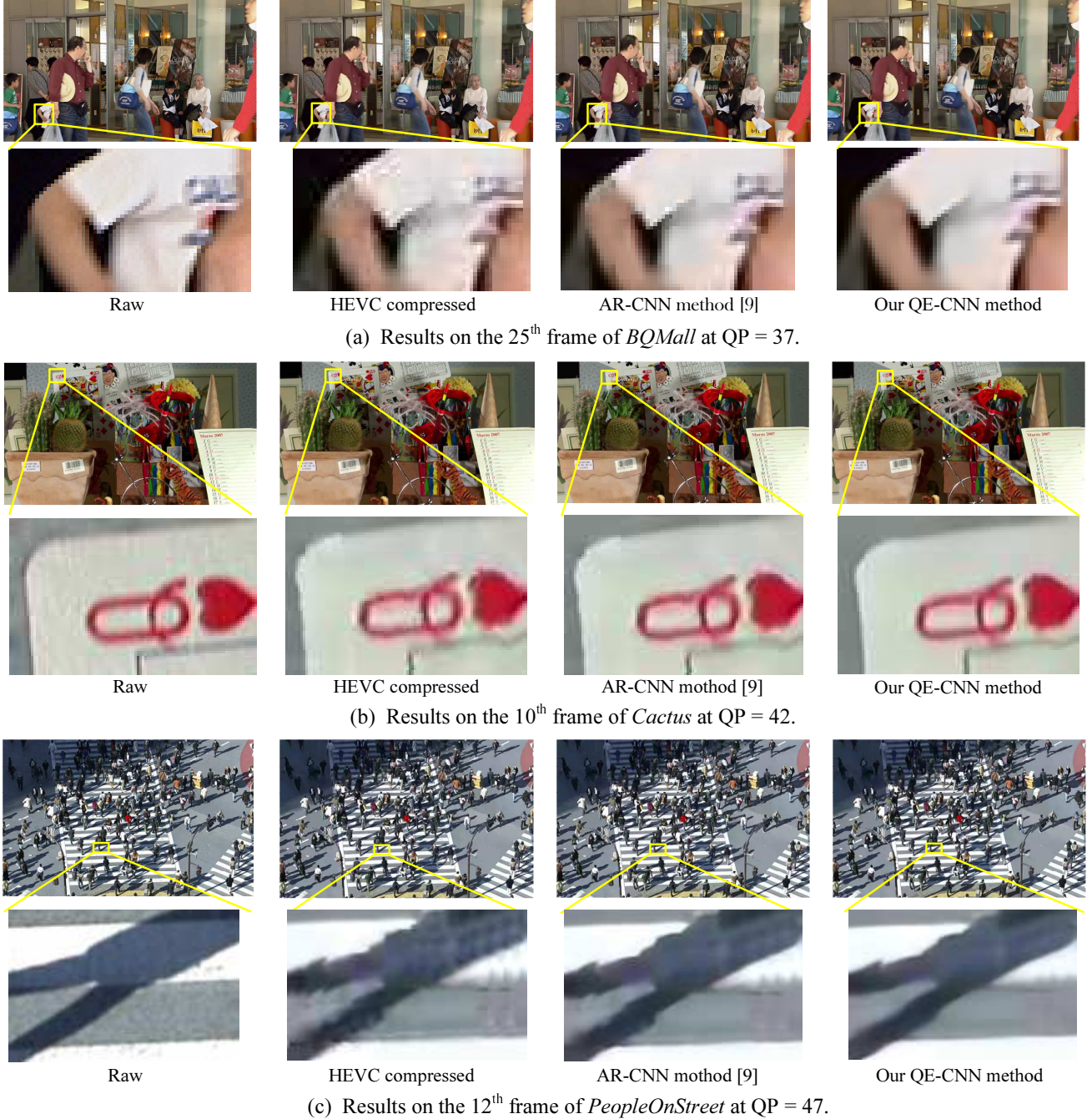


Fig. 3. Subjective results of our QE-CNN and AR-CNN [9] methods on three frames at QP = 37, 42 and 47.

C. Computational time analysis

Moreover, we evaluate the computational time of our QE-CNN method for quality enhancement compared to the conventional AR-CNN [9]. In our experiments, we evaluate the computational time via the running time of quality enhancement on an Ubuntu PC equipped with one GeForce GTX 1080 GPU. Fig. 4 shows the computational time of our QE-CNN method and the conventional AR-CNN method, as well as their Y-PSNR improvement. Note that the results in this figure are obtained by averaging over all the test sequences.

As shown in Fig. 4, our QE-CNN method performs con-

siderably better than the conventional AR-CNN method in terms of Y-PSNR improvement. However, this improvement occurs at the expense of computational time. Specifically, the running time of AR-CNN method is 0.70 ms per Coding Tree Unit (CTU). In contrast, our QE-CNN-I model requires approximately 1.53 ms per CTU, and QE-CNN-P consumes 3.90 ms per CTU. Thus, the performance improvement of our QE-CNN method is at the expense of computational time. The next section primarily focuses on enabling a trade-off between quality enhancement and computational time when applying our QE-CNN method.

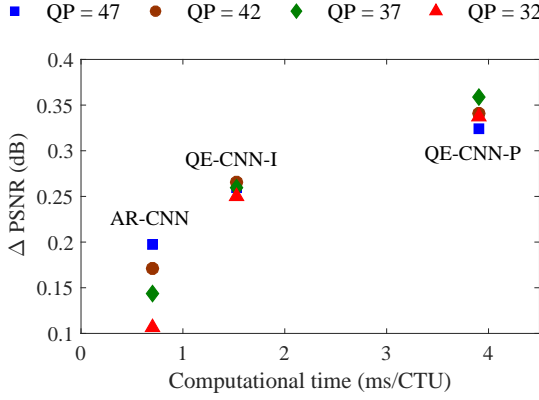


Fig. 4. Computational time versus quality enhancement for our QE-CNN and AR-CNN [9] methods.

V. TIME-CONSTRAINED QUALITY ENHANCEMENT OPTIMIZATION

As discussed in Section IV-C, our QE-CNN method may consume large amounts of computational time for enhancing the quality of HEVC videos, especially for high-resolution videos or with insufficient computational resources. Meanwhile, in many application scenarios, e.g., real-time video play, quality enhancement has to be constrained by a time limitation. Hence, we propose the TQEo scheme, i.e., time-constrained quality enhancement optimization scheme, enabling our QE-CNN method to be practical for time-constrained scenarios.

A. Formulation for TQEo scheme

To meet the time constraint, the computational time of our QE-CNN method needs to be reduced. The computational time can be reduced by applying QE-CNN to only some of the CTUs at a frame. Interestingly, we find that the quality enhanced by our QE-CNN method varies across different CTUs. To quantify this variation, we evaluate the Relative Standard Deviations (RSDs) of the MSE reduction among CTUs at a frame when applying our QE-CNN method. Note that RSD is the ratio of standard deviation divided by the corresponding mean value. For each sequence, the RSD of the MSE reduction is averaged over all frames. As shown in Fig. 5, the RSD of the MSE reduction is approximately or even greater than 100% for all 17 test sequences. In other words, the standard deviation is comparable to its corresponding mean value. This result indicates a large difference in quality enhancement across different CTUs. Therefore, under the time constraint, our QE-CNN method needs to be conducted on CTUs that may achieve large quality enhancement, in order to maximize the quality enhancement.

Our TQEo scheme aims to control the computational time of our QE-CNN method through a constraint while optimizing quality enhancement. The formulation of our TQEo scheme can be modeled as

$$\max_{\{k_n\}_{n=1}^N} \sum_{n=1}^N \Delta \text{MSE}_n(k_n) \quad \text{s.t.} \quad \sum_{n=1}^N t_n(k_n) \leq T, \quad (15)$$

where $\Delta \text{MSE}_n(k_n)$ is defined as the MSE reduction of the n -th CTU and $t_n(k_n)$ is the computational time for quality

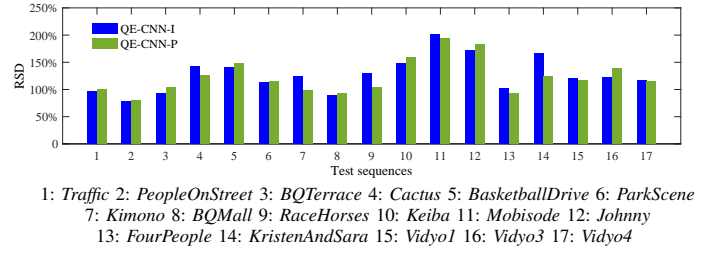


Fig. 5. RSD of the MSE reduction across CTUs in each test sequence. For each sequence, the RSD of the MSE reduction is averaged over all frames. Note that all test sequences are compressed by HEVC LDP mode at QP = 42, and then QE-CNN is applied for quality enhancement.

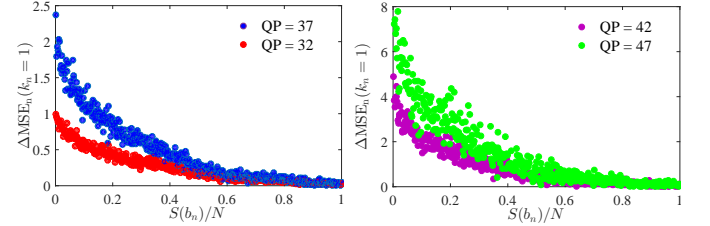


Fig. 6. Relationship between $\Delta \text{MSE}_n(k_n)$ and $S(b_n)/N$ for I frames. Note that $\Delta \text{MSE}_n(k_n)$ for each $S(b_n)$ is averaged among all training sequences in this figure.

enhancement on the n -th CTU. Here, $k_n \in \{0, 1, 2\}$ is a variable to be calculated for solving (15). In particular, $k_n = 0$ means that the n -th CTU is without any quality enhancement, $k_n = 1$ stands for applying QE-CNN-I in the CTU, and $k_n = 2$ indicates applying QE-CNN-P. Additionally, T denotes the time constraint, and N is the total number of CTUs at a frame. Next, we discuss the solution to our TQEo formulation for I and P frames, respectively.

B. Solution to (15) for I frames

To solve (15) for I frames, we first model $t_n(k_n)$ and $\Delta \text{MSE}_n(k_n)$ by training on 10 sequences randomly selected from our dataset introduced in Section III-C. Note that these 10 training sequences do not overlap with all the 17 test sequences of Sections IV and VI. Recall that only the network of QE-CNN-I can be used on I frames; thus, $k_n \in \{0, 1\}$ for I frames. Clearly, we have $t_n(k_n = 1) = 0$ when the CTU is without any quality enhancement. For modeling $t_n(k_n = 1)$, we record the computational time of QE-CNN-I among all CTUs of the training sequences when running on a computer with one GeForce GTX 1080 GPU. Consequently, the mean and standard deviation of $t_n(k_n = 1)$ are 1.536 ms and 0.096 ms, respectively. Since the standard deviation is significantly smaller than the mean value for $t_n(k_n = 1)$, we simply set $t_n(k_n = 1)$ as a constant 1.536 ms in our TQEo scheme. Thus, given the constraint of $\sum_{n=1}^N t_n(k_n) \leq T$ in (15), we can obtain that the number of CTUs with $k_n = 1$ at a frame is equivalent to

$$N_1 = \lfloor T/t_n(k_n = 1) \rfloor, \quad (16)$$

where $\lfloor \cdot \rfloor$ represents rounding down. In the following, we model $\Delta \text{MSE}_n(k_n)$ to solve the optimization problem of $\max \sum_{n=1}^N \Delta \text{MSE}_n(k_n)$ for (15).

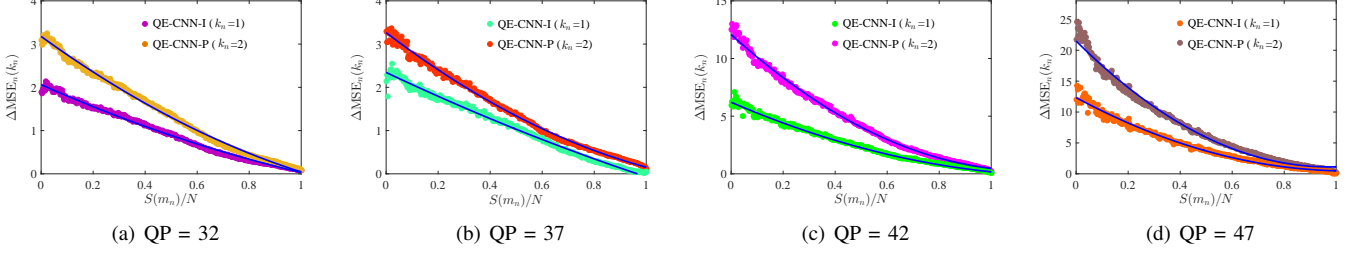


Fig. 7. Relationship modeling of $\Delta\text{MSE}_n(k_n)$ for P frames. Note that the points of $\Delta\text{MSE}_n(k_n)$ for each $S(m_n)$ are the average values among all the frames in the 10 training sequences.

TABLE VII
COEFFICIENTS IN THE FUNCTION OF $\Delta\text{MSE}_n(k_n)$.

| QP | 32 | 37 | 42 | 47 |
|-----------------|--------------|--------------|--------------|--------------|
| a_1 | 0.643 | 0.429 | 3.693 | 10.85 |
| b_1 | 2.672 | 2.841 | 9.728 | 22.71 |
| c_1 | 2.061 | 2.344 | 6.266 | 12.34 |
| R-Square | 0.995 | 0.994 | 0.995 | 0.990 |
| a_2 | 1.218 | 1.476 | 8.928 | 21.64 |
| b_2 | 4.352 | 4.588 | 20.54 | 42.00 |
| c_2 | 3.177 | 3.265 | 12.08 | 21.50 |
| R-Square | 0.997 | 0.996 | 0.996 | 0.990 |

For I frames, we find that $\Delta\text{MSE}_n(k_n)$ of different CTUs has a strong correlation with their corresponding bit allocation in HEVC, denoted by b_n . The Spearman correlation coefficients between $\Delta\text{MSE}_n(k_n)$ and b_n , averaged over all training sequences, are 0.85, 0.80, 0.73 and 0.65 for QP = 32, 37, 42 and 47, respectively. Additionally, as shown in Fig. 6, $S(b_n)$ is denoted as the rank of descending sorted $\{b_n\}_{n=1}^N$ in a frame³, and $\Delta\text{MSE}_n(k_n)$ reduces along with the descending b_n . Therefore, at I frames, CTUs with more allocated bits are more likely to achieve higher quality enhancement, and they should be with high priority in enhancing quality under the time constraint. Thus, given $N_1 = \lfloor T/t_n(k_n = 1) \rfloor$, the solution to (15) can be obtained as

$$k_n = \begin{cases} 1, & S(b_n) \leq N_1, \\ 0, & S(b_n) > N_1, \end{cases} \quad (17)$$

for I frames of HEVC compressed videos.

C. Solution to (15) for P frames

To solve (15) for P frames, we model $t_n(k_n)$ and $\Delta\text{MSE}_n(k_n)$ of (15) as follows. First, the computational time of QE-CNN-I on P frames is the same as that on I frames; thus, $t_n(k_n = 1) = 1.536$ ms still holds for P frames. Similarly, QE-CNN-P consumes 3.900 ms per CTU on average, with a small deviation of 0.120 ms. Thus, $t_n(k_n = 2)$ is also set by a constant, i.e., 3.900 ms.

Next, we focus on modeling $\Delta\text{MSE}_n(k_n)$ for HEVC P frames. Here, Mean Absolute Deviation (MAD) is used to predict the potential quality enhancement of $\Delta\text{MSE}_n(k_n)$ at

TABLE VIII
SOLUTION TO (19) FOR 1080P SEQUENCES.

| T/T_{\max} | QP = 32 | | QP = 37 | | QP = 42 | | QP = 47 | |
|--------------|---------|-------|---------|-------|---------|-------|---------|-------|
| | N_1 | N_2 | N_1 | N_2 | N_1 | N_2 | N_1 | N_2 |
| 10% | 121 | 0 | 121 | 0 | 119 | 1 | 119 | 1 |
| 20% | 241 | 1 | 243 | 0 | 132 | 44 | 165 | 31 |
| 30% | 259 | 42 | 325 | 16 | 132 | 92 | 142 | 88 |
| 40% | 231 | 101 | 292 | 77 | 132 | 140 | 132 | 140 |
| 50% | 203 | 160 | 246 | 143 | 114 | 195 | 132 | 188 |
| 60% | 170 | 221 | 198 | 210 | 109 | 245 | 114 | 243 |
| 70% | 137 | 282 | 142 | 280 | 99 | 297 | 109 | 293 |
| 80% | 99 | 345 | 81 | 352 | 86 | 350 | 109 | 341 |
| 90% | 58 | 409 | 0 | 432 | 66 | 406 | 76 | 402 |

each CTU⁴ because it is strongly correlated with $\Delta\text{MSE}_n(k_n)$, as discussed in the following. We define m_n as the MAD value of the n -th CTU, and $S(m_n)$ is the rank of the descending sort of $\{m_n\}_{n=1}^N$ within a frame. Fig. 7 shows the relationship between $S(m_n)$ and $\Delta\text{MSE}_n(k_n)$ over all training sequences. Here, we apply the normalized index $S(m_n)/N$ as the horizontal axis in Fig. 7, such that the relationship between $\Delta\text{MSE}_n(k_n)$ and $S(m_n)/N$ is suitable for different resolutions (with different numbers of CTUs). From Fig. 7, two facts can be observed: 1) $\Delta\text{MSE}_n(k_n = 1)$ and $\Delta\text{MSE}_n(k_n = 2)$ both decrease along with decreasing m_n , and 2) $\Delta\text{MSE}_n(k_n = 2)$ decreases faster than $\Delta\text{MSE}_n(k_n = 1)$ with decreasing m_n . Accordingly, we need to set a larger k_n for CTUs with larger m_n . That is, the values of k_n can be set as

$$k_n = \begin{cases} 2, & S(m_n) \leq N_2, \\ 1, & N_2 < S(m_n) \leq N_1 + N_2, \\ 0, & S(m_n) > N_1 + N_2, \end{cases} \quad (18)$$

where N_1 and N_2 represent the numbers of CTUs with $k_n = 1$ and $k_n = 2$, respectively. Given (18), formulation (15) can be rewritten as follows:

$$\begin{aligned} \max_{N_1, N_2} \quad & \sum_{S(m_n)=1}^{N_2} \Delta\text{MSE}_n(k_n = 2) + \sum_{S(m_n)=N_2+1}^{N_2+N_1} \Delta\text{MSE}_n(k_n = 1) \\ \text{s.t.} \quad & N_1 \cdot t_n(k_n = 1) + N_2 \cdot t_n(k_n = 2) \leq T. \end{aligned} \quad (19)$$

³Descending sort consumes only 0.020 ms per 1080p frame by an Intel Core(TM) i7-4790K CPU, which can be ignored in our TQEo scheme.

⁴It consumes 0.492 ms to calculate MADs for all CTUs in a 1080p frame using an Intel Core(TM) i7-4790K CPU. Thus, it takes much less time than QE-CNN.

TABLE IX
RESULTS OF TIME CONTROL ACCURACY FOR OUR TQE0 SCHEME.

| | | QP = 32 | | | | QP = 37 | | | | QP = 42 | | | | QP = 47 | | | |
|------------------------|------------------------|---------|-------|-------|-------|---------|-------|-------|-------|---------|-------|-------|-------|---------|-------|-------|-------|
| T/T _{max} (%) | | 20 | 40 | 60 | 80 | 20 | 40 | 60 | 80 | 20 | 40 | 60 | 80 | 20 | 40 | 60 | 80 |
| A | <i>Traffic</i> | 20.11 | 40.20 | 60.16 | 80.08 | 20.10 | 40.24 | 60.21 | 80.10 | 19.04 | 39.99 | 60.00 | 79.99 | 19.66 | 40.16 | 60.12 | 80.13 |
| | <i>PeopleOnStreet</i> | 20.12 | 40.12 | 60.09 | 80.05 | 20.08 | 40.23 | 60.22 | 80.09 | 19.93 | 39.97 | 59.99 | 79.98 | 20.09 | 40.11 | 60.21 | 80.09 |
| B | <i>BQTerrace</i> | 20.21 | 40.18 | 60.15 | 80.08 | 20.16 | 40.31 | 60.25 | 80.11 | 19.93 | 39.95 | 60.00 | 79.98 | 20.11 | 40.09 | 60.02 | 79.97 |
| | <i>Cactus</i> | 20.18 | 40.18 | 60.15 | 80.09 | 20.16 | 40.22 | 60.16 | 80.04 | 19.88 | 39.97 | 59.95 | 79.95 | 20.12 | 40.12 | 60.10 | 80.12 |
| C | <i>BasketballDrive</i> | 20.17 | 40.20 | 60.13 | 80.09 | 20.15 | 40.20 | 60.18 | 80.04 | 19.92 | 39.96 | 59.98 | 79.90 | 20.13 | 40.15 | 60.10 | 80.06 |
| | <i>ParkScene</i> | 20.14 | 40.20 | 60.14 | 80.09 | 20.12 | 40.23 | 60.18 | 80.08 | 19.95 | 39.98 | 59.98 | 80.00 | 20.09 | 40.13 | 60.07 | 80.11 |
| D | <i>Kimono</i> | 20.15 | 40.20 | 60.17 | 80.12 | 20.14 | 40.23 | 60.16 | 80.04 | 19.95 | 39.97 | 59.97 | 79.91 | 20.13 | 40.11 | 60.06 | 80.03 |
| | <i>BQMall</i> | 20.25 | 40.26 | 60.25 | 80.14 | 20.20 | 40.09 | 60.19 | 80.04 | 19.53 | 39.91 | 59.90 | 79.93 | 20.23 | 40.44 | 60.31 | 80.06 |
| E | <i>RaceHorses</i> | 20.15 | 40.00 | 60.01 | 79.98 | 20.26 | 39.98 | 60.00 | 79.78 | 18.11 | 39.29 | 59.91 | 79.95 | 18.87 | 38.89 | 59.97 | 80.08 |
| | <i>Keiba</i> | 20.23 | 40.10 | 60.22 | 80.04 | 20.29 | 40.09 | 60.20 | 80.01 | 19.24 | 39.94 | 59.92 | 79.92 | 19.72 | 40.41 | 60.32 | 80.08 |
| F | <i>Mobisode</i> | 20.16 | 40.08 | 60.14 | 79.98 | 20.21 | 40.13 | 60.22 | 80.00 | 19.20 | 39.89 | 59.89 | 79.93 | 19.70 | 40.51 | 60.34 | 80.14 |
| | <i>Johnny</i> | 20.11 | 40.11 | 60.14 | 80.04 | 20.06 | 40.22 | 60.15 | 80.08 | 19.96 | 39.99 | 59.98 | 79.99 | 20.07 | 40.15 | 60.09 | 80.07 |
| G | <i>FourPeople</i> | 20.21 | 40.30 | 60.40 | 80.45 | 20.07 | 40.22 | 60.07 | 80.07 | 19.94 | 40.00 | 60.00 | 80.03 | 20.08 | 40.15 | 60.11 | 80.07 |
| | <i>KristenAndSara</i> | 20.13 | 40.15 | 60.15 | 80.04 | 20.02 | 40.22 | 60.15 | 80.10 | 19.98 | 40.03 | 59.99 | 80.00 | 20.09 | 40.14 | 60.07 | 80.06 |
| H | <i>Vidyo1</i> | 19.98 | 40.06 | 60.10 | 80.07 | 20.00 | 40.23 | 60.15 | 80.11 | 19.94 | 40.00 | 59.98 | 79.97 | 19.12 | 39.88 | 59.77 | 79.65 |
| | <i>Vidyo3</i> | 20.08 | 40.08 | 60.04 | 80.01 | 20.06 | 40.21 | 60.08 | 80.09 | 19.88 | 39.97 | 59.95 | 80.01 | 19.64 | 40.08 | 60.04 | 80.01 |
| | <i>Vidyo4</i> | 20.11 | 40.11 | 60.10 | 80.06 | 20.03 | 40.22 | 60.11 | 80.07 | 19.95 | 39.98 | 59.97 | 79.98 | 20.07 | 40.13 | 60.06 | 80.06 |
| Average MAE (%) | | 0.149 | 0.149 | 0.150 | 0.087 | 0.124 | 0.195 | 0.158 | 0.077 | 0.333 | 0.075 | 0.039 | 0.039 | 0.266 | 0.241 | 0.134 | 0.092 |

Then, to obtain the function of $\Delta\text{MSE}_n(k_n)$ in (19), we utilize least-squares fitting of the second-order polynomial regression, and the fitting function is obtained as follows:

$$\Delta\text{MSE}_n(k_n = 1) = a_1 \left(\frac{S(m_n)}{N} \right)^2 - b_1 \frac{S(m_n)}{N} + c_1, \quad (20)$$

$$\Delta\text{MSE}_n(k_n = 2) = a_2 \left(\frac{S(m_n)}{N} \right)^2 - b_2 \frac{S(m_n)}{N} + c_2, \quad (21)$$

where a_1, a_2, b_1, b_2, c_1 and c_2 are the coefficients presented in Table VII. Table VII also reports that all the R-square values of the fitting are above 0.99, verifying the effectiveness of fitting functions (20) and (21).

Given (20) and (21), the problem of (19) is a non-linear integer optimization problem. Therefore, we apply the branch-and-bound algorithm [37] to solve (19). To avoid the overhead computational time consumed by solving formulation (19), we establish a look-up table for the solutions to (19) at each specific T . Then, given T , we can simply obtain N_1 and N_2 by table look-up. Table VIII presents the solution for 1080p sequences as an example of the table look-up. In Table VIII, we use T/T_{\max} instead of T as the target. Note that $T_{\max} = N \cdot t_n(k_n = 2)$ is the maximum time of our TQE0 scheme, which applies QE-CNN to all CTUs. Additionally, T_{\max} is a constant for each specific video. That is, the constraint in (19) can be represented by

$$\frac{N_1}{N} \cdot \frac{t_n(k_n = 1)}{t_n(k_n = 2)} + \frac{N_2}{N} \leq \frac{T}{T_{\max}} \quad (22)$$

for establishing the look-up table. The reason is that the values of $t_n(k_n = 1)$ and $t_n(k_n = 2)$ may vary among different devices, but $t_n(k_n = 1)/t_n(k_n = 2) \approx 0.394$ is almost unchanged. Therefore, T/T_{\max} in Table VIII makes

the solution more general for different devices⁵.

Finally, the solution to (15) can be obtained for the P frames of HEVC compressed videos. As a result, the computational time for quality enhancement can be controlled for both I and P frames with maximal enhancement on video quality.

VI. EXPERIMENTS FOR OUR TQE0 SCHEME

In this section, we validate the performance of our TQE0 scheme from the aspects of both control accuracy and quality enhancement evaluated under different time constraints. The experiments are conducted on an Ubuntu PC with one GeForce GTX 1080 GPU. The HEVC test sequences are the same as in Section IV.

A. Accuracy of computational time control

We now evaluate the accuracy of computational time control of our TQE0 scheme to validate its effectiveness in controlling the time to a constraint. Since no other work focuses on time control of quality enhancement, we do not compare the control accuracy with other methods. Table IX presents the time control accuracy of our TQE0 scheme. In Table IX, we present the results of actual time divided by the maximum time T_{\max} . As shown in Table IX, the control error is up to 1.89% (*RaceHorses*, QP = 42, 20%), and most of the errors are less than 0.200%. Table IX also tabulates the Mean Absolute Error (MAE), which is calculated as

$$\text{MAE} = \frac{|\Delta T|}{T_{\max}}, \quad (23)$$

averaged over all the test sequences. Here, ΔT indicates the error between the target and actual time. It is apparent that the

⁵In our experiments, we tested $t_n(k_n = 1)/t_n(k_n = 2)$ on three different devices, which are equipped with a GeForce GTX TITAN GPU, GeForce GTX 1080 GPU and GeForce GTX 1080 Ti GPU, respectively. We found that the values of $t_n(k_n = 1)/t_n(k_n = 2)$ are all within the range of 0.393 ~ 0.395. Moreover, in practice, T_{\max} can be simply estimated by recording the computational time of QE-CNN-P on a few CTUs.

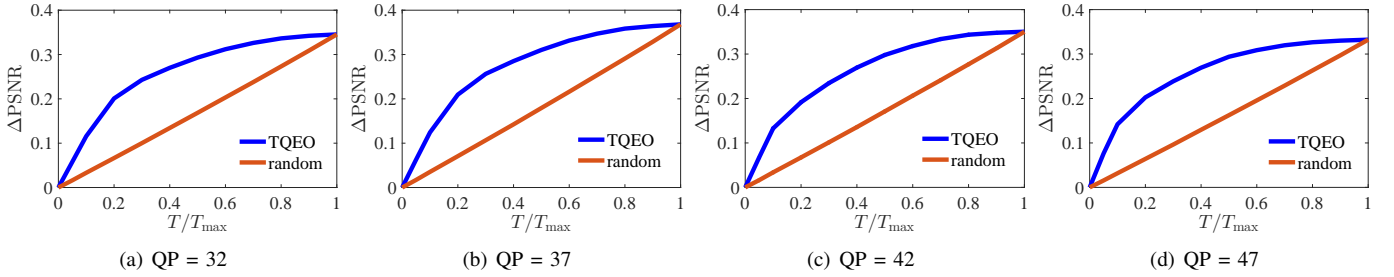


Fig. 8. Time-constrained quality enhancement performance averaged among all the test sequences.

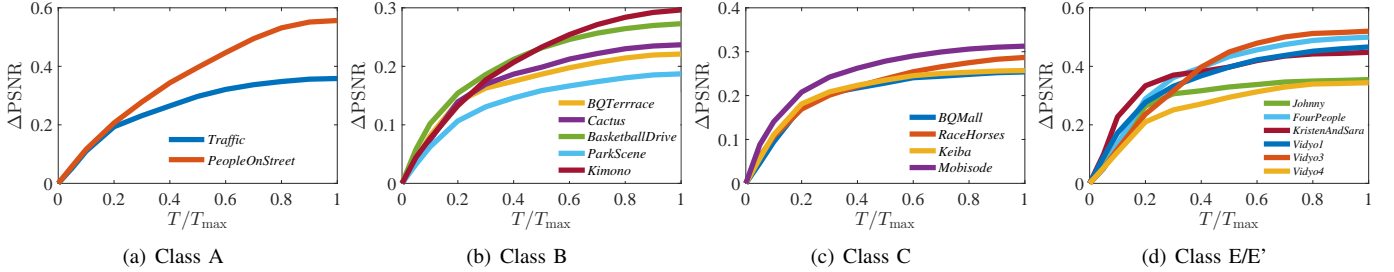


Fig. 9. Time-constrained quality enhancement performance on each test sequence at QP = 32.

average MAEs of our TQEO scheme in most cases are below 0.150%, and the highest value of MAE is only 0.333%. In conclusion, our TQEO scheme performs well in controlling the computational time of quality enhancement under a time constraint.

B. Quality enhancement under different time constraints

Next, we focus on assessing the quality enhancement of our TQEO scheme under different time constraints. As in Section IV, quality enhancement is measured in terms of Y-PSNR improvement (Δ PSNR). We compare the Δ PSNR of our TQEO scheme with a baseline that applies the QE-CNN method on randomly selected CTUs. Fig. 8 shows the Δ PSNR averaged among all 17 test sequences, along with different time constraints. As shown, under each time constraint, our TQEO scheme achieves a higher Δ PSNR than the baseline. Specifically, the average Δ PSNR of our TQEO scheme reaches 58.2% of the maximum Δ PSNR at QP = 32, with only 20% of the computational time of T_{\max} . When the time constraint is half of T_{\max} , our TQEO scheme is able to improve the Y-PSNR by 0.2931 dB on average, which is 84.9% of the maximum Δ PSNR. Moreover, Fig. 9 presents the results on all test sequences at QP = 32. Similar to the average Δ PSNR curves, we can observe that the curves are up-convex for quality enhancement under different time constraints. Consequently, the quality enhancement of our TQEO scheme significantly outperforms the baseline of enhancing randomly selected CTUs, whose Δ PSNR is almost linearly related to T . That is, our TQEO scheme succeeds in optimizing the quality enhancement given the limited computational time.

C. Implementation

Finally, we design a prototype to achieve real-time quality enhancement of HEVC compressed videos by using our TQEO scheme. Our prototype is implemented on an Ubuntu PC

with four GeForce GTX 1080 GPUs. In our prototype, the computational time target T in formulation (15) needs to satisfy the real-time constraint⁶, e.g., $T = 16.67$ ms per each frame for 60 Hz sequences.

We evaluate the performance of our prototype on 10 test sequences. The duration of each test sequence is 10 s. Table X presents the actual computational time and quality enhancement for our prototype. We can observe that the actual time used for quality enhancement satisfies the real-time constraint. Moreover, the control error of the computational time is very small, which is up to 0.19 s, far less than the video duration of 10 s. The average control error is only 0.073 s, i.e., 0.73% of the 10 s duration. Fig. 10 shows the computational time of our prototype at each frame of sequences *RaceHorses*, *FourPeople*, *Keiba* and *Johnny*. As shown in Fig. 10, the frame-level control error of our prototype is also small, indicating high fluency when displaying the enhanced HEVC videos.

The quality enhancement performance is shown in Table X. As shown, at QP = 47, our prototype has a 0.2458 dB Δ PSNR on 480p@30 Hz sequences on average (*RaceHorses*, *Keiba* and *Mobisode*), and it achieves 0.1493 dB on the 480p@60 Hz sequence (*BQMall*). For 720p@60 Hz (Class E/E') sequences, the Δ PSNR is 0.1534 dB on average at QP = 47. Similar results can be found for the other QPs. Furthermore, our prototype can achieve BD-rate savings of up to 6.83%, and an average of 6.34% for 480p@30 Hz sequences, in our real-time prototype. The BD-rate savings for 720p@60 Hz (Class E/E') sequences is 2.80% on average when achieving real-time enhancement. To summarize, our prototype is effective in both time control accuracy and quality enhancement for HEVC compressed videos in the real-time implementation.

⁶Note that we did not take the decoding time into consideration in our prototype, because the latest HEVC decoder achieves very fast decoding. For example, the decoder proposed in [38] is able to decode HEVC LDP videos at a speed of 4 Gpixels/s (0.14 s for a 10 s 720p@60 Hz sequence).

TABLE X
PERFORMANCE OF OUR PROTOTYPE.

| Class | Sequence | Actual time (s) | | | | Δ PSNR (dB) | | | | BD-rate (%) |
|-------|-----------------------|-----------------|---------|---------|---------|--------------------|---------|---------|---------|-------------|
| | | QP = 32 | QP = 37 | QP = 42 | QP = 47 | QP = 32 | QP = 37 | QP = 42 | QP = 47 | |
| C | <i>RaceHorses</i> | 9.81 | 9.81 | 9.81 | 9.83 | 0.2169 | 0.2262 | 0.2121 | 0.2117 | -6.8282 |
| | <i>Keiba</i> | 9.93 | 9.93 | 9.87 | 9.86 | 0.2211 | 0.2320 | 0.2290 | 0.3010 | -6.1855 |
| | <i>Mobisode</i> | 9.93 | 9.91 | 9.97 | 9.71 | 0.2580 | 0.2714 | 0.2274 | 0.2248 | -5.9942 |
| | <i>BQMall</i> | 9.98 | 9.97 | 9.94 | 10.0 | 0.1654 | 0.1774 | 0.1427 | 0.1493 | -3.8446 |
| E/E' | <i>Johnny</i> | 9.90 | 10.0 | 9.91 | 9.90 | 0.1026 | 0.1154 | 0.1107 | 0.1992 | -2.8413 |
| | <i>FourPeople</i> | 9.91 | 9.97 | 9.90 | 9.99 | 0.0956 | 0.1119 | 0.1392 | 0.1011 | -2.4498 |
| | <i>KristenAndSara</i> | 9.88 | 9.99 | 9.91 | 10.0 | 0.1754 | 0.2284 | 0.2531 | 0.2617 | -4.8185 |
| | <i>Vidyo1</i> | 9.97 | 10.0 | 9.99 | 10.0 | 0.1356 | 0.1409 | 0.1533 | 0.1622 | -3.0907 |
| | <i>Vidyo3</i> | 10.0 | 9.98 | 9.99 | 10.0 | 0.0887 | 0.0674 | 0.0565 | 0.0729 | -1.4138 |
| | <i>Vidyo4</i> | 9.92 | 9.88 | 9.88 | 10.0 | 0.0823 | 0.0873 | 0.1021 | 0.1231 | -2.2120 |

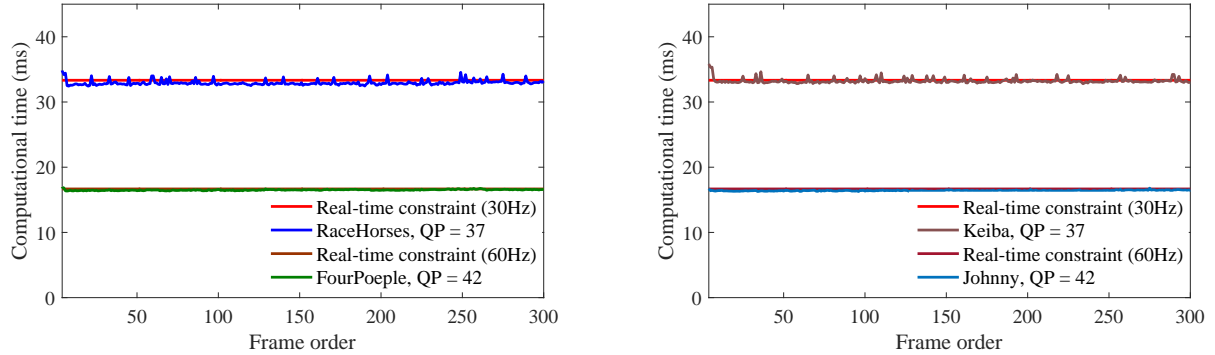


Fig. 10. Frame-level computational time of our prototype on four test sequences.

VII. CONCLUSION

This paper has proposed the QE-CNN method at the decoder side, to improve the quality of HEVC videos. Our QE-CNN method learns to reduce the artifacts of both intra- and inter-mode compression, rather than only reducing intra-mode compression artifacts in the existing CNN-based quality enhancement methods. Specifically, two networks, i.e., QE-CNN-I and QE-CNN-P, were proposed to learn the features of intra- and inter-mode distortion, respectively. As such, our QE-CNN method can enhance the quality for both I and P frames of HEVC compressed videos. The experimental results have shown that the proposed QE-CNN method is able to advance the state-of-the-art quality enhancement of HEVC videos.

However, the QE-CNN method introduces heavy computational complexity. To make the quality enhancement adaptive to different time constraints, we further proposed the TQEo scheme for controlling the computational time of our QE-CNN method. We first established the TQEo formulation, which maximizes the enhanced quality under a time constraint by selecting some of the CTUs for quality enhancement. Then, two solutions were derived for the established formulation for the I and P frames of HEVC compressed videos. The experimental results verified the effectiveness of the proposed TQEo scheme in terms of control accuracy and quality enhancement. Finally, a prototype was established to implement our TQEo scheme in a real-time application of quality enhancement.

Our work, at the current stage, only focuses on enhancing the quality of HEVC videos with LDP mode. An interesting future work is to further implement our QE-CNN method for other coding modes, and even other video coding standards. This may be achieved by re-training our proposed QE-CNN

network on other types of videos. Besides, real-time enhancement requires a large amount of computational resources in our prototype. Thus, another future work is accelerating the proposed QE-CNN method and applying our TQEo scheme on other hardware platforms, e.g., FPGA, mobile, and so forth.

REFERENCES

- [1] G. J. Sullivan, J.-R. Ohm, W.-J. Han, and T. Wiegand, “Overview of the high efficiency video coding (HEVC) standard,” *IEEE TCSVT*, pp. 1649–1668, 2012.
- [2] T. K. Tan, R. Weerakkody, M. Mrak, N. Ramzan, V. Baroncini, J. R. Ohm, and G. J. Sullivan, “Video quality evaluation methodology and verification testing of hevc compression performance,” *IEEE TCSVT*, pp. 76–90, Jan 2016.
- [3] A.-C. Liew and H. Yan, “Blocking artifacts suppression in block-coded images using overcomplete wavelet representation,” *IEEE TCSVT*, pp. 450–461, 2004.
- [4] A. Foi, V. Katkovnik, and K. Egiazarian, “Pointwise shape-adaptive DCT for high-quality denoising and deblocking of grayscale and color images,” *IEEE TIP*, 2007.
- [5] J. Jancsary, S. Nowozin, and C. Rother, “Loss-specific training of non-parametric image restoration models: A new state of the art,” in *ECCV*, 2012.
- [6] H. Chang, M. K. Ng, and T. Zeng, “Reducing artifacts in JPEG decompression via a learned dictionary,” *IEEE TSP*, pp. 718–728, 2014.
- [7] C. Jung, L. Jiao, H. Qi, and T. Sun, “Image deblocking via sparse representation,” *Signal Processing: Image Communication*, pp. 663–677, 2012.
- [8] C. Wang, J. Zhou, and S. Liu, “Adaptive non-local means filter for image deblocking,” *Signal Processing: Image Communication*, pp. 522–530, 2013.
- [9] C. Dong, Y. Deng, C. Change Loy, and X. Tang, “Compression artifacts reduction by a deep convolutional network,” in *ICCV*, 2015.
- [10] Z. Wang, D. Liu, S. Chang, Q. Ling, and T. S. Huang, “D3: Deep dual-domain based fast restoration of JPEG-compressed images,” *arXiv preprint arXiv:1601.04149*, 2016.
- [11] Y. LeCun, L. Bottou, Y. Bengio, and P. Haffner, “Gradient-based learning applied to document recognition,” *Proceedings of the IEEE*, pp. 2278–2324, 1998.

- [12] Q. Han and W.-K. Cham, "High performance loop filter for HEVC," in *ICIP*, 2015.
- [13] J. Zhang, C. Jia, N. Zhang, S. Ma, and W. Gao, "Structure-driven adaptive non-local filter for high efficiency video coding (HEVC)," in *DCC*, 2016.
- [14] W.-S. Park and M. Kim, "CNN-based in-loop filtering for coding efficiency improvement," in *IVMSP*, 2016.
- [15] Y. Dai, D. Liu, and F. Wu, "A convolutional neural network approach for post-processing in hevc intra coding," in *MMM*, 2017.
- [16] R. Yang, M. Xu, and Z. Wang, "Decoder-side HEVC quality enhancement with scalable convolutional neural network," in *Multimedia and Expo (ICME), 2017 IEEE International Conference on*. IEEE, 2017, pp. 817–822.
- [17] A. Krizhevsky, I. Sutskever, and G. E. Hinton, "Imagenet classification with deep convolutional neural networks," in *NIPS*, 2012.
- [18] A. Karpathy, G. Toderici, S. Shetty, T. Leung, R. Sukthankar, and L. Fei-Fei, "Large-scale video classification with convolutional neural networks," in *CVPR*, 2014.
- [19] R. Girshick, J. Donahue, T. Darrell, and J. Malik, "Rich feature hierarchies for accurate object detection and semantic segmentation," in *CVPR*, 2014.
- [20] J. Long, E. Shelhamer, and T. Darrell, "Fully convolutional networks for semantic segmentation," in *CVPR*, 2015.
- [21] C. Dong, C. L. Chen, K. He, and X. Tang, "Learning a deep convolutional network for image super-resolution," in *ECCV*, 2014.
- [22] S. Li, C. Zhu, Y. Gao, Y. Zhou, F. Dufaux, and M.-T. Sun, "Lagrangian multiplier adaptation for rate-distortion optimization with inter-frame dependency," *IEEE TCSVT*, pp. 117–129, 2016.
- [23] Y. Gao, C. Zhu, S. Li, and T. Yang, "Temporal dependent rate-distortion optimization for low-delay hierarchical video coding," *IEEE TIP*, 2017.
- [24] G. Corrêa, P. Assuncao, L. Agostini, and L. A. da Silva Cruz, "Complexity control of high efficiency video encoders for power-constrained devices," *IEEE TCE*, pp. 1866–1874, 2011.
- [25] X. Deng, M. Xu, S. Li, and Z. Wang, "Complexity control of hevc based on region-of-interest attention model," in *VCIP*, 2014.
- [26] X. Deng, M. Xu, L. Jiang, X. Sun, and Z. Wang, "Subjective-driven complexity control approach for HEVC," *IEEE TCSVT*, pp. 91–106, 2016.
- [27] M. J. Langroodi, J. Peters, and S. Shirmohammadi, "Decoder-complexity-aware encoding of motion compensation for multiple heterogeneous receivers," *ACM TOMM*, p. 46, 2015.
- [28] R. Yang, M. Xu, L. Jiang, and Z. Wang, "Subjective-quality-optimized complexity control for hevc decoding," in *Multimedia and Expo (ICME), 2016 IEEE International Conference on*. IEEE, 2016, pp. 1–6.
- [29] R. Yang, M. Xu, Z. Wang, and X. Tao, "Saliency-guided complexity control for hevc decoding," *arXiv preprint arXiv:1610.02516*, 2016.
- [30] P. Arbelaez, M. Maire, C. Fowlkes, and J. Malik, "Contour detection and hierarchical image segmentation," *IEEE TPAMI*, pp. 898–916, 2011.
- [31] G. K. Wallace, "The JPEG still picture compression standard," *IEEE TCE*, pp. xviii–xxiv, 1992.
- [32] K. He, X. Zhang, S. Ren, and J. Sun, "Delving deep into rectifiers: Surpassing human-level performance on imagenet classification," in *ICCV*, 2015.
- [33] M. D. Zeiler and R. Fergus, "Visualizing and understanding convolutional networks," in *ECCV*, 2014.
- [34] K. He, X. Zhang, S. Ren, and J. Sun, "Deep residual learning for image recognition," in *CVPR*, 2015.
- [35] J. Kim, J. K. Lee, and K. M. Lee, "Accurate image super-resolution using very deep convolutional networks," in *CVPR*, 2016.
- [36] F. Bossen *et al.*, "Common test conditions and software reference configurations," *Joint Collaborative Team on Video Coding (JCT-VC), JCTVC-L1100*, 2011.
- [37] D. Li and X. Sun, *Nonlinear integer programming*. Springer Science & Business Media, 2006.
- [38] D. Zhou, S. Wang, H. Sun, J. Zhou, J. Zhu, Y. Zhao, J. Zhou, S. Zhang, S. Kimura, T. Yoshimura *et al.*, "14.7 A 4Gpixel/s 8/10b H. 265/HEVC video decoder chip for 8K ultra HD applications," in *ISSCC*. IEEE, 2016, pp. 266–268.